In-situ microscale through-silicon via strain measurements by synchrotron x-ray microdiffraction exploring the physics behind data interpretation

Xi Liu, Paragkumar A. Thadesar, Christine L. Taylor, Hanju Oh, Martin Kunz, Nobumichi Tamura, Muhannad S. Bakir, and Suresh K. Sitaraman

Citation: Applied Physics Letters **105**, 112109 (2014); doi: 10.1063/1.4896141
View online: http://dx.doi.org/10.1063/1.4896141
View Table of Contents: http://scitation.aip.org/content/aip/journal/apl/105/11?ver=pdfcov
Published by the AIP Publishing

In-situ microscale through-silicon via strain measurements by synchrotron x-ray microdiffraction exploring the physics behind data interpretation

Xi Liu,[1,2] Paragkumar A. Thadesar,[2] Christine L. Taylor,[1] Hanju Oh,[2] Martin Kunz,[3] Nobumichi Tamura,[3] Muhannad S. Bakir,[2] and Suresh K. Sitaraman[1]
[1]*The George W. Woodruff School of Mechanical Engineering, Georgia Institute of Technology, Atlanta, Georgia 30332, USA*
[2]*School of Electrical and Computer Engineering, Georgia Institute of Technology, Atlanta, Georgia 30332, USA*
[3]*Advanced Light Source, Lawrence Berkeley National Laboratory Berkeley, California 94720, USA*

(Received 4 June 2014; accepted 8 September 2014; published online 19 September 2014)

In-situ microscale thermomechanical strain measurements have been performed in combination with synchrotron x-ray microdiffraction to understand the fundamental cause of failures in microelectronics devices with through-silicon vias. The physics behind the raster scan and data analysis of the measured strain distribution maps is explored utilizing the energies of indexed reflections from the measured data and applying them for beam intensity analysis and effective penetration depth determination. Moreover, a statistical analysis is performed for the beam intensity and strain distributions along the beam penetration path to account for the factors affecting peak search and strain refinement procedure. © *2014 AIP Publishing LLC*. [http://dx.doi.org/10.1063/1.4896141]

Interconnects have emerged as a key bottleneck for system performance leading to the growing focus towards 2.5-dimensional (2.5D) and 3-dimensional (3D) integration of chips.[1] Through-silicon vias (TSVs) are key enablers to 2.5D and 3D integration. The coefficient of thermal expansion (CTE) mismatch between the silicon and copper in TSVs leads to thermomechanical reliability concerns.[2] To address these concerns with TSVs and find potential solutions, various characterization techniques have been utilized in the literature: indentation techniques, micro-Raman spectroscopy, bending beam technique, and synchrotron x-ray microdiffraction (mXRD). Indentation techniques measure local stresses in silicon and copper using normal load induced by the residual stress but knowledge of a known stress-free state is required.[3] Micro-Raman spectroscopy measures local stresses near the surface of silicon using the shift in the frequency of an impinging laser but cannot measure the stress in the copper.[4,5] Bending beam technique measures the stress in silicon and copper using the curvature of a wafer but only gives stresses averaged across the wafer.[6] Synchrotron x-ray microdiffraction measures local stresses in silicon and copper using raster scans of TSVs, and consequently is a more attractive technique. However, since the strain distribution along the x-ray penetration depth direction in the TSVs is averaged and projected as 2D strain maps, the data interpretation is challenging using the obtained 2D strain maps.[7] Although depth-resolved x-ray microdiffraction techniques such as differential aperture x-ray microscopy do not have the data interpretation issue, data collection would take an extortionate amount of time to map the entire sample.[8,9] To bypass data interpretation concerns, Murray *et al.* performed strain measurements of TSVs formed in a silicon-on-insulator (SOI) wafer and focused only on the 0.5 μm thin silicon layer of the SOI wafer for strain analysis.[10] To interpret the raster scanned 2D strain maps, a beam intensity based averaging method was demonstrated in earlier work,[11] in which the whole beam spectrum from 5 keV to 22 keV was used for the beam intensity calculation without considering the energies corresponding to indexed reflections of the material of interest. Consequently, a more effective and accurate data interpretation method is needed to better understand the physics behind the synchrotron mXRD measurements and data analysis.

To better capture the physics behind the raster scan and data analysis, this paper presents a data averaging technique with the assistance of finite-element modeling (FEM). In this technique, the energies of indexed reflections are obtained from the measurement data and applied for beam intensity analysis. Also, factors affecting peak search and strain refinement procedure are considered by statistically analyzing the beam intensity and strain distributions along the beam penetration path, correlating their effect with peak broadening, peak search, and strain refinement.

The synchrotron mXRD test was carried out on beamline 12.3.2 (Ref. 12) at the Advanced Light Source (ALS), Lawrence Berkeley National Laboratory (LBNL). To perform the measurements, 60 μm diameter and 300 μm tall TSVs at a 150 μm pitch were fabricated with 1 μm thick silicon dioxide liner between the silicon and copper. The fabricated wafer with TSVs was then diced into small coupons and cross-section polished until 31 μm silicon remained in front of the TSVs, which preserves the TSV/silicon mechanical boundary condition while still small enough for synchrotron x-rays to penetrate through. Next, the coupons were mounted on a heating stage with scanning plane facing the incident beam at 45°, as shown in Fig. 1. Scans were conducted at 150 °C using a focused 1 μm × 1 μm size polychromatic x-ray beam (beam energy range of 5 keV to 22 keV) to measure the deviatoric strains $\varepsilon'_{ij} = \varepsilon_{ij} - \delta I_{ij}$, where $\delta = (\varepsilon_{xx} + \varepsilon_{yy} + \varepsilon_{zz})/3$.

Fig. 2 shows the measured 2D deviatoric strain maps of silicon around two adjacent TSVs. Here, silicon was selected as the material of interest because critical failures in TSV's are mainly cohesive cracks in silicon and interfacial separation between the copper and the silicon.[2] Also, clearer strain

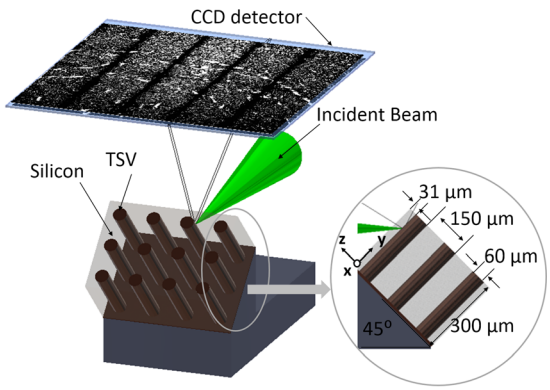

FIG. 1. Schematic of setup for the strain measurements of TSVs using synchrotron mXRD.

distribution trends of silicon can be easily determined and used for model validation as well as critical location identification. As discussed earlier, the 2D strain maps actually represent 3D strain distributions in the silicon surrounding the TSVs. Moreover, when x-rays penetrate a significant distance into silicon, they get attenuated due to photoelectric absorption, scattering, and pair production. Consequently, to obtain meaningful conclusions from the measured 2D strain maps of the silicon surrounding TSVs, answers to the following questions are critical: How is the effective penetration depth determined and how is the strain information along the effective penetration depth represented?

The first question deals with the determination of effective penetration depth. X-ray photons with different energies have different penetration depths, whereas the effective penetration depth can be defined as the distance from the front surface to where the intensity of x-rays falls to $1/e$ of its value at the surface, where e is the Euler's number. This value is commonly referred to as attenuation length, which is a materials' property dependent on x-ray energy, material chemical composition, and density. Photons with lower energy decay with a shorter effective penetration depth, and have contribution only for the shallower penetration depth. A prior work observed that high energy photons ($\geq$15 keV) of the applied white beam dominate the final 2D strain maps of silicon.[11] The study in this paper finds that the observation in earlier work[11] is due to fact that energies of the majority of indexed reflections of silicon correspond to photon energies higher than 15 keV, as shown in Figs. 3 and 4. Thus, the obtained 2D strain maps (Fig. 2) actually represent the strain information from x-rays extending a significant distance into the silicon. Consequently, the energies of the indexed reflections with the corresponding mass attenuation coefficients are utilized for the calculation of the beam intensity along the penetration path and to investigate the effective penetration depth.

The second question is how the 3D strain information along the effective penetration depth is represented in the final 2D strain maps. To address this, the correlation of the beam intensity and strain distribution to the peak search and strain refinement is analyzed.

With respect to beam intensity, as indexation is based on the most intense reflections observed, it is reasonable to assume that the major components of the collected information are from the front section along the effective penetration depth. The reason for this can be explained by examining the

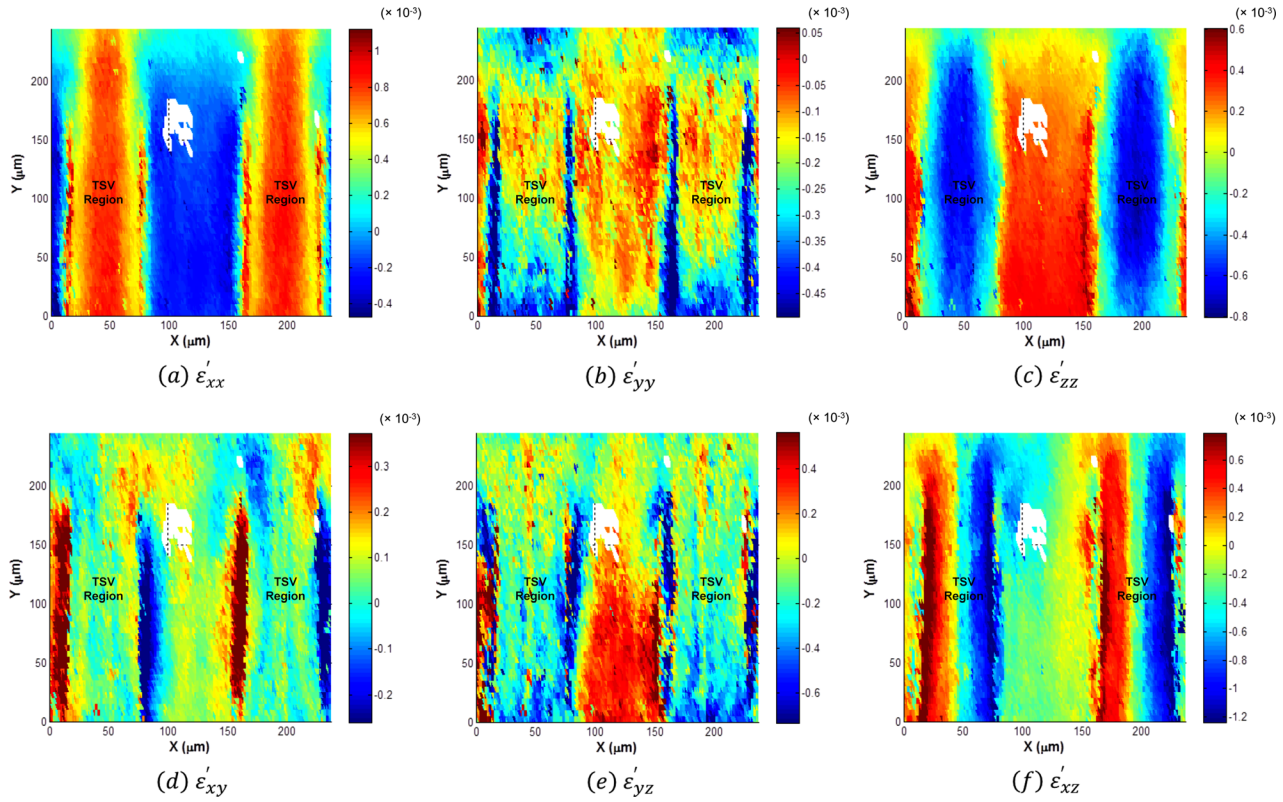

FIG. 2. Measured deviatoric strain distribution maps of the silicon surrounding TSVs at 150 °C (the white patches are due to the missing data points during raster scan of TSVs, and they do not impact the overall TSV strain trends).

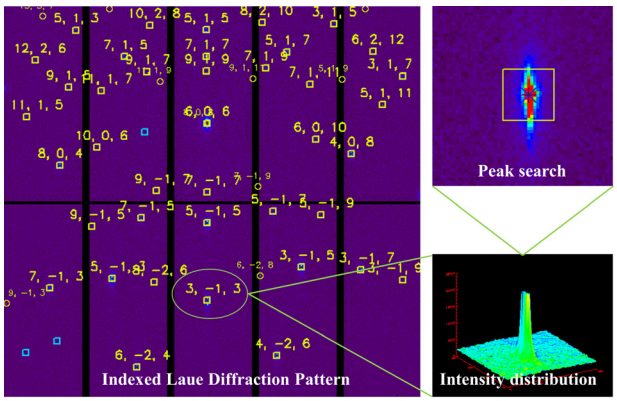

FIG. 3. Example indexed Laue diffraction pattern of silicon.

peak search procedure using x-ray microdiffraction analysis software (XMAS):[13] First, the XMAS program performs background fitting and subtracting on the collected Laue diffraction pattern. Next, XMAS identifies the locations with the maximum intensity in each intensity island (Fig. 3), and then chooses appropriate fitting algorithms to determine the exact peak locations. This procedure indicates that high intensity regions of the reflections generally determine the locations of the peaks and thus the strains. Therefore, the strains near the front section of the sample should have greater contribution on the final 2D strain maps, which also suggests that there should be a relationship between the beam intensities and the contributions to the final 2D strain maps. Thus, a weighted function based on the intensities of the beam along the penetration direction is developed to account for the contributions.

In addition to beam intensity, the effect of strain distribution on peak search and deviatoric strain refinement is another factor that needs to be considered. As shown in Fig. 3, asymmetric peak broadening (streaking) occurs at some of the reflections, which means that the crystal lattice associated to them is imperfect.[14–16] For single crystal silicon, the broadening is mainly caused by non-uniform distribution of lattice strains along the beam penetration path. The asymmetric reflection broadening is given by $\beta_s = \xi \tan\theta$ (ξ is the integral breath of the strain distribution; θ is the Bragg angle).[15] Since the diffraction angle is a function of lattice strain ($\varepsilon_l = -\cot\theta_o \Delta\theta$), there is an intensity maxima in each intensity island (Fig. 3). This maxima corresponds to the majority of lattice strains in the same range along the penetration path which contributed the most to the signal. On the other hand, because the deviatoric strain tensors are obtained by fitting a large number of reflections (≥ 6),[13,17] they reflect a weighted average value obtained over not only the probed depth but also from the majority lattice strains. Therefore, the effect of the strain distribution on the peak search and deviatoric strain refinement can be represented in the model by statistical analysis of the deviatoric strains along the penetration depth and filtering strains corresponding to lower intensities, which have negligible contributions to peak location determination and thus deviatoric strain calculation. The details about how to realize it in the model is discussed in the following modeling paragraph.

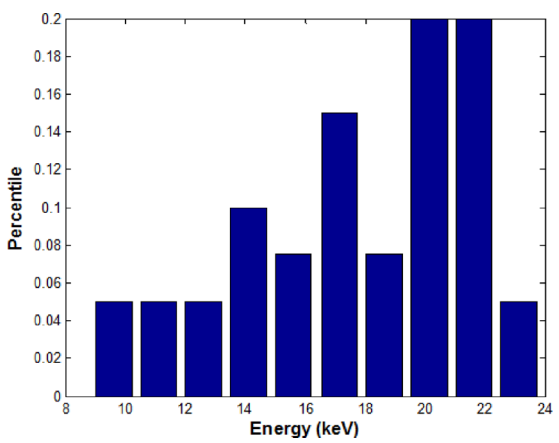

FIG. 4. Distribution of energies of example indexed reflections of silicon.

Based on the above discussion, addressing the determination of the effective penetration depth, and the strain information representation along the effective penetration depth at each data position, an energy absorption based data averaging method is proposed with the assistance of FEM to interpret the 2D strain maps, as shown in Fig. 5. First, the energies of the indexed reflections of silicon are calculated and input into the proposed data averaging model to calculate the beam intensities in the silicon, and only the beam intensity larger than $1/e$ of its value at the surface are considered. Simultaneously, a finite-element TSV array model is built with the same geometry as the tested TSV sample. To simulate the sequential fabrication process, all the materials are activated sequentially at their process stress-free temperature through the ANSYS™ element birth-and-death approach. Thereafter, the following data processing steps are carried out: (I) Reading out deviatoric strain in the silicon from the model and calculating beam intensity along the penetration depth, as the example shown in Fig. 6(a). (II) Statistical analysis of the strain distribution along the effective penetration depth and sorted strains into equally spaced segments, as shown in Fig. 6(c). As seen, the

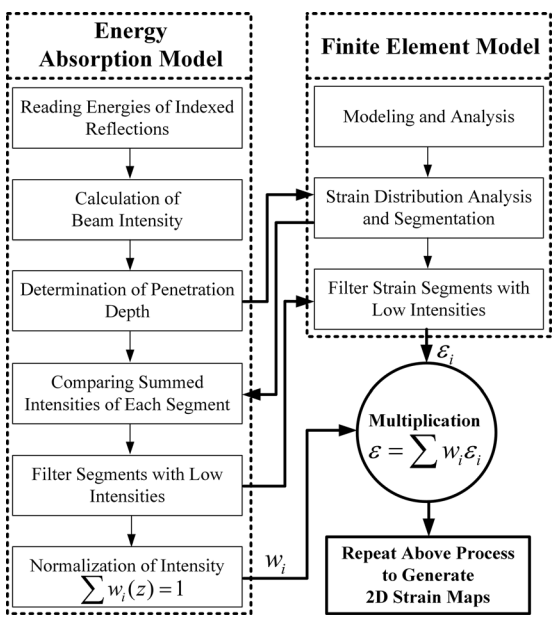

FIG. 5. Process flow of proposed data averaging method based on the energy dependent x-ray absorption.

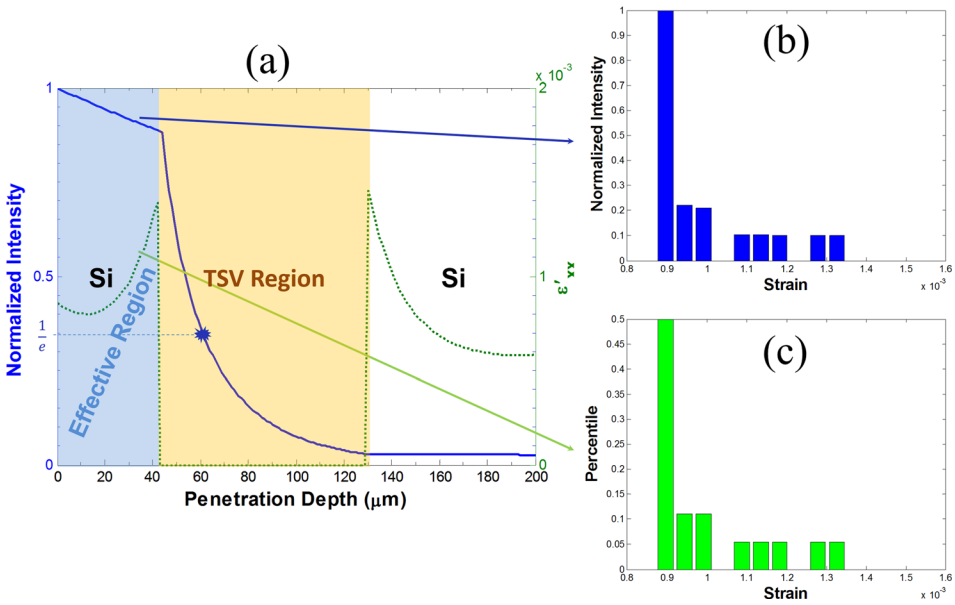

FIG. 6. Example beam intensity and deviatoric strain ε'_{xx} of silicon along the penetration depth passing the TSV centers in (a) and (b) histogram of beam intensity, and (c) histogram of strain ε'_{xx} in the effective region.

effective penetration depth of the example in Fig. 6 is smaller than that defined by beam intensity larger than $1/e$ because the beam passes the TSV center and only the silicon is the material of interest. (III) Summing corresponding beam intensities of each segment (Fig. 6(b)). (IV) Analyzing the distribution of the intensities of each segment and identifying segments with low intensities, which have negligible contribution to peak location determination. Figs. 6(b) and 6(c) suggest that the distribution of intensities is in line with the distribution of ε'_{xx}. This is also true for other strain components. (V) Filtering corresponding strains in segments with lower intensities. Beam intensities corresponding to the remaining strain data points along the penetration path are normalized to form the beam intensity based weight function $w(z)$, where $\sum w_i(z) = 1$. This is based on the assumption that the contribution of the collected data to the final 2D strain maps depends on the magnitudes of the beam intensity along the penetration direction. (VI) The remaining strain values are multiplied by the aforementioned beam intensity based weight

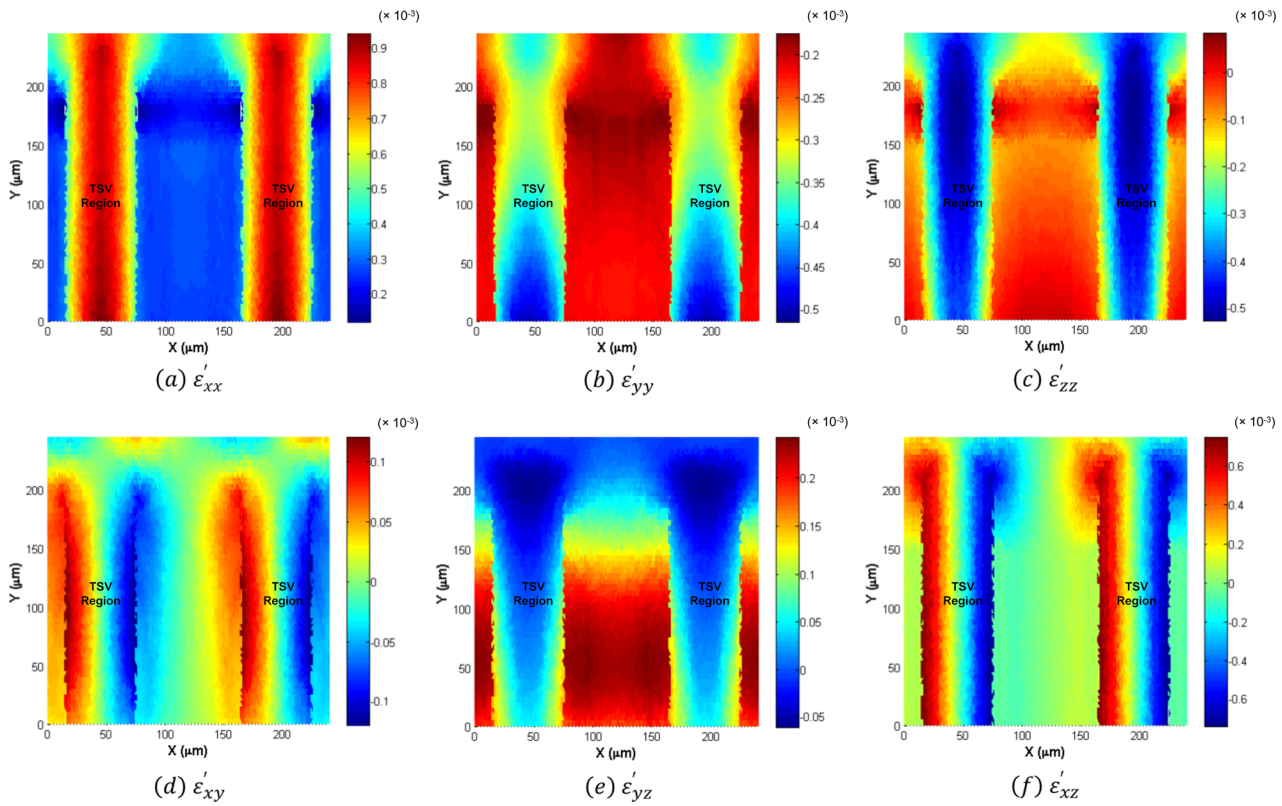

FIG. 7. Model predicted deviatoric strain distribution maps of silicon at 150 °C.

function ($\varepsilon = \sum w_i \varepsilon_i$) to get a strain value at any given point on the scanning plane. This process is repeated until all the points on the scanning plane are covered.

Fig. 7 plots the model predicted six deviatoric strain components. Compared to the measured strain maps in Fig. 2, it shows that the model predicts the strain distributions of all six deviatoric strain components with the local details. Yet, there are some scattered highly strained points in the measured strain maps, which cannot be captured by the model. This is because the through-silicon hole etching with Bosch process results in sidewall with scallops[18] which are not considered in the FEM model. Moreover, copper vias expand and tend to extrude outward at high temperatures, resulting in large local deformations on the scalloped sidewalls. Additionally, the surface scratches, and thus the resulting residual stresses on the front surface due to cross-section polishing, are difficult to capture in the model. However, these discrepancies do not affect the overall strain distribution, and thus, the TSV critical location determination. Moreover, capturing the trend validates the proposed methodology for data interpretation, which can be applied to future raster scan strain data analysis.

In summary, to interpret the synchrotron XRD measured 2D strain distribution maps, which present the TSV 3D strain distribution, this paper has proposed data averaging method based on the energy dependent x-ray absorption and explored the physics behind the peak search and strain refinement procedure. Penetration depth analysis indicates that the final 2D strain maps are projected strains up to a significant distance along the penetration depth into the silicon due to majority of indexed reflections of silicon corresponding to high energy spectrums. Moreover, strain analysis results show that the proposed method predicts the trend of the strain distribution, which validates the proposed data analysis methodology.

This work was supported by the Semiconductor Research Corporation under Contract No. 2012-KJ-2255. The Advanced Light Source (ALS) is supported by the Director, Office of Science, Office of Basic Energy Sciences, of the U.S. Department of Energy under Contract No. DE-AC02-05CH11231 at the Lawrence Berkeley National Laboratory (LBNL).

[1]J. U. Knickerbocker, P. S. Andry, B. Dang, R. R. Horton, M. J. Interrante, C. S. Patel, R. J. Polastre, K. Sakuma, R. Sirdeshmukh, E. J. Sprogis, S. M. Sri-Jayantha, A. M. Stephens, A. W. Topol, C. K. Tsang, B. C. Webb, and S. L. Wright, IBM J. Res. Dev. **52**, 553 (2008).
[2]X. Liu, Q. Chen, V. Sundaram, R. R. Tummala, and S. K. Sitaraman, Microelectron. Reliab. **53**(1), 70 (2013).
[3]G. Lee, M. Choi, S. Jeon, K. Byun, and D. Kwon, in *Proceedings of the 62nd IEEE Electronic Components and Technology Conference, San Diego, CA, 29 May–1 June 2012* (IEEE, 2012), pp. 781–786.
[4]D. Wolf, V. Simons, V. Cherman, R. Labie, B. Vandevelde, and E. Beyne, in *Proceedings of the 62nd IEEE Electronic Components and Technology Conference, San Diego, CA, 29 May–1 June 2012* (IEEE, 2012), pp. 331–337.
[5]S. Ryu, Q. Zhao, M. Hecker, H. Son, K. Byun, J. Im, P. S. Ho, and R. Huang, J. Appl. Phys. **111**(6), 063513 (2012).
[6]S. Ryu, T. Jiang, K. H. Lu, J. Im, H. Son, K. Byun, R. Huang, and P. S. Ho, Appl. Phys. Lett. **100**(4), 041901 (2012).
[7]A. S. Budiman, H. A. S. Shin, B. J. Kim, S. H. Hwang, H. Y. Son, M. S. Suh, Q. H. Chung, K. Y. Byun, N. Tamura, M. Kunz, and Y. C. Joo, Microelectron. Reliab. **52**(3), 530 (2012).
[8]B. C. Larson, W. Yang, G. E. Ice, J. D. Budai, and J. Z. Tischler, Nature **415**, 887 (2002).
[9]W. Yang, B. C. Larson, J. Z. Tischler, G. E. Ice, J. D. Budai, and W. Liu, Micron **35**(6), 431 (2004).
[10]C. E. Murray, T. Graves-Abe, R. Robison, and Z. Cai, Appl. Phys. Lett. **102**(25), 251910 (2013).
[11]X. Liu, P. A. Thadesar, C. L. Taylor, M. Kunz, N. Tamura, M. S. Bakir, and S. K. Sitaraman, Appl. Phys. Lett. **103**(2), 022107 (2013).
[12]M. Kunz, N. Tamura, C. Kai, A. A. MacDowell, R. S. Celestre, M. M. Church, S. Fakra, E. E. Domning, J. M. Glossinger, J. L. Kirschman, G. Y. Morrison, D. W. Plate, B. V. Smith, T. Warwich, V. V. Yashchuk, H. A. Padmore, and E. Ustundag, Rev. Sci. Instrum. **80**(3), 035108 (2009).
[13]R. Barabash and G. Ice, *Strain and Dislocation Gradients from Diffraction: Spatially-Resolved Local Structure and Defects* (Imperial College Press, United Kingdom, 2014).
[14]T. Ungar, Scr. Mater. **51**(8), 777 (2004).
[15]G. Williamson and W. Hall, Acta Metall. **1**(1), 22 (1953).
[16]A. S. Budiman, W. D. Nix, N. Tamura, B. C. Valek, K. Gadre, J. Maiz, R. Spolenak, and J. R. Patel, Appl. Phys. Lett. **88**(23), 233515 (2006).
[17]J.-S. Chung and G. E. Ice, J. Appl. Phys. **86**(9), 5249 (1999).
[18]Y.-C. Hsin, C.-C. Chen, J. H. Lau, P.-J. Tzeng, S.-H. Shen, Y.-F. Hsu, S.-C. Chen, C.-Y. Wn, J.-C. Chen, T.-K. Ku, and M.-J. Kao, in *Proceedings of the 61st IEEE Electronic Components and Technology Conference*, Lake Buena Vista, FL, 31 May–3 June 2011 (IEEE, 2011), pp.1130–1135.